Structural analysis of FRP parts from waste wind turbine blades for building reuse applications

Lawrence C. Bank & Franco R. Arias

City College of New York, City University of New York, New York, USA

T. Russell Gentry, Tristan Al-Haddad & Benjamin Tasistro-Hart Georgia Institute of Technology, Atlanta, USA

Jian-Fei Chen Queen's University Belfast, Belfast, UK

ABSTRACT: The focus of this work is on the problem of the future waste to be generated by the decommissioning of wind farms and especially the Fiber Reinforced Polymer (FRP) composite materials used in the wind turbine blades. The FRP composites used to manufacture the blades are not biodegradable and present severe problems with regard to waste management and their End-of-Life (EOL). The impact on polymers on the environment and society has become a major concern in many countries. With the increased awareness of the environmental impacts of climate change, decreased and more expensive natural resources, and greater global concerns for health, the barriers to FRP production and waste disposal are likely to increase. In the context of the circular economy the preferred method to manage FRP waste is to use it in new applications or processes. Recent structural analysis research conducted by the authors related to reuse of FRP composite material parts from decommissioned wind turbine blades in infrastructure applications is presented in this paper.

1 INTRODUCTION

Fiber Reinforced Polymer (FRP) composite materials are not biodegradable and present unique problems with regard to waste management and their End-of-Life (EOL). The impact on polymers on the environment and society has become a major concern for many countries. Legislation in Europe has been enacted to restrict the disposal of non-biodegradable polymers (including FRPs) in landfills. A number of EU Horizon 2020 projects have recently been awarded in this area. In the US landfilling (aka dumping or tipping) is the predominant method of disposing of FRP scrap and waste costing in the range of \$45 to \$200 per ton. With the increased awareness of the environmental impacts of climate change, decreased and more expensive natural resources, and greater global concerns for health, the barriers to FRP production and waste disposal are likely to increase. Since the 1990s, there has been a developing body of research that has studied the issues of recycling of FRP composites. There are three primary methods to dispose of FRP composites at the present time, (1) landfilling, (2) incineration, and, (3) reusing all or part of the composite material in a secondary process or application. A fourth method, which is being explored quite actively in the carbonfiber composite industry is (4) reclamation, where the original constituent fiber and matrix materials are recovered for reuse. In the context of the circular economy the preferred method to dispose of FRP waste is to use it in new application or processes which needs to be conducted using a life- cycle-assessment (LCA) methodology.

Recent analyses of the key issues related to the EOL of FRP wind turbine blades can be found in Liu and Barlow (2017), Jensen and Skelton (2018) and Bank et al. (2018). For example, a typical 2.0 MW turbine with three 50 m blades has approximately 20 tonnes of FRP material and an 8 MW turbine has approximately 80 tonnes of FRP material (based on a conservative 1 MW \approx 10 tonnes of FRP). Based on predicted (moderate growth scenario) future wind power installations from the Global Wind Energy Council (GWEC) a total of 16.8 million tonnes will need to be managed globally by 2030 and 39.8 million tonnes by 2050 (Bank et al, 2018). Innovative design and logistical concepts for reusing and recycling these blades, from whole blades to sub-structural parts to granular materials and powders, must be developed and implemented to keep wind energy sustainable.

Recent reviews of recycling of FRP composites are provided in Oliveux et al., (2015) and Job et al, (2016). Two methods to dispose of FRP composites are used at the present: disposal in landfills or incineration (with or without energy recovery and subsequent disposal of the residual ash or reuse

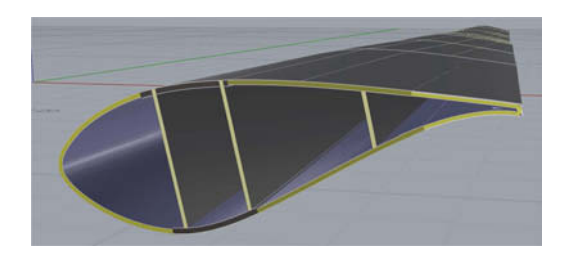


Figure 1. Cross-sectional view of 100 m blade.

as a precursor for cement production in a cement kiln). Jensen & Skelton (2018) propose the following categorization of second-life options for FRP products: Reuse/Repurpose, Resize/Reshape, Recycle, Recover/Convert. Recover/Convert consists of reclamation of the constituent fibers or the resins by thermo-chemical methods or production of syngas fuels. Recycling consists of shredding or grinding the FRP material into granular material as filler for use in concrete or other composites (see review by Yazdanbakhsh & Bank, 2014), or cutting the FRP material into small pieces for use as large aggregates in concrete (Yazdanbakhsh et al, 2018), Reuse/Repurpose consists of reusing the entire FRP blade and Resize/Reshape consists of reusing large parts of the blade in new products (Jensen & Skelton, 2018; Bank et al, 2018).

In what follows the structural analysis of Resize/Reshape part from a 100 m long of a FRP blade as an element for a large roof frame is described.

2 REUSE OF PARTS OF FRP BLADES AS STRUCTURAL ELEMENTS IN BUILDINGS

2.1 Reuse concepts from parts a 100 m blade

A number of potential architectural and structural applications of parts taken from a 100 m long wind blade designed by Sandia National Laboratories (SNL) are described in Bank et al (2018). SNL-100-01 is a publically-available 100 meter long prototype wind turbine blade model (Griffith, 2013). It has glass fiber reinforced polymer (GFRP) in the shell structure and webs, and carbon fiber reinforced polymer (CFRP) composite material in the spar caps. The geometry is defined by 25 different airfoil shapes. The materials are defined by 393 different solid and sandwich composite material lay-ups. The software packages Numerical Manufacturing and Design Tool (NuMAD) (Berg & Resor, 2012) and RHINO 3D (www.rhino3d.com) were used to build three-dimensional models of the blade. A cross-section of the model blade looking down towards the blade tip is shown in Fig. 1

The blade has a foam core shell, three internal foam core webs (identified as 1,2 and 3 from left to right in Fig. 1) and a carbon fiber spar cap (shown in black above and below the webs 1 and 2). The SNL-100-01 blade was chosen for preliminary modeling and conceptual studies since its geometry and materials are available. Commercial blade data is proprietary hence

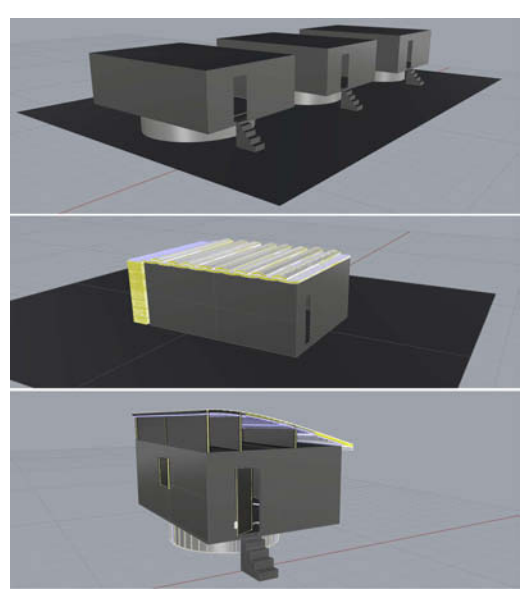


Figure 2. Reuse concepts from 100 m long blade parts.

geometric and material data is not available which makes modeling for reuse significantly more difficult and is a subject of current research (Tasistro-Hart et al, 2019). In addition, the 100 m long blade (which is similar in size to current production offshore wind turbine blades) which has a width of 7.63 m at maximum chord and is useful for conceptual exercises as it can be divided up into large structural parts for possible reuse in structural applications. Designs for platform foundations (from root section), doors and window shutters (from webs), roofing beams (from the shell) and roof frames (from the shell and webs) for a 5 m by 7 m (35 m²) CMU block house are shown in Fig. 2. (Bank et al, 2018.)

The roof frame concept was chosen for further detailed structural analysis.

2.1.1 *Material properties and loads*

The mechanical (stiffness and strength) and physical (density) properties of the materials as well as the layups used in the SNL-100-01 blade are given in Griffith (2013). Different layups and materials are used for different locations around the cross-section and along the length of the blade, the leading edge panels, the trailing edge panels, the webs and the spar caps. The relevant properties for the roof panel were extracted from a segment between 27.6 m and 35.8 m from the root end (where the blade is attached to the hub). Table 1 lists the properties of the different materials used in the blade (Griffith, 2013).

Using the layup schedules provided in Griffith (2013) the properties of the different laminates and sandwich panels used in the roof frame were determined and used in both hand calculations and finite element analysis (FEA). It should be noted that residual properties, assuming the blade would be in service for 20-25 years, were not considered at this time.

Table 1. Material properties

	E ₁₁ GPa				ρ kg/m³		
Foam	0.27	0.27	0.02	0.3	200		
Glass	41.8	14.0	2.63	0.28	1920	972	702
UD [0] 2							
SNLBiax	13.6	13.3	11.8	0.49	1780	144	213
$[\pm 45]_4$							
SNLTriax	27.7	13.7	7.20	0.39	1850		
$[\pm 45]_4[0]_2$							
SNLCarbon	114.5	8.39	5.99	0.27	1220	1546	1571
(UD/Biax)							

The 16.6 MN weight of the roof frame was distributed over the entire projected roof area (34.6 m²) to give a distributed load dead load (DL) of 0.48 kN/m². A typical roof live load (LL) of 0.96 kN/m² was assumed. The total gravity load (DL+LL) applied to the roof frame was 1.44 kN/m². Load factors were not applied.

2.1.2 Hand calculations

Hand calculations using one-dimensional mechanics of materials models were used to determine: (1) The flexural stresses in the wide sandwich skin panel in the transverse direction between webs 2 and 3, and (2) the flexural stresses in web 2 in the longitudinal direction (bending about its strong axis in the horizontal plane).

Case (1): The sandwich skin panel consist of a 60 mm thick foam core and two 5 mm face skins of SNL Triax glass fiber composite. Since this panel is in the transverse (contour) orientation relative to the blade longitudinal axis the transverse properties of the materials are used. $E_{T(triax)} = 13.65 \text{ GPa}, E_{foam} = 0.256$ GPa. The panel length (between webs 2 and 3) is 2.04 m and a unit width is assumed for one way bending. The skin panel is conservatively considered to be simply supported at the web junctions. The maximum midspan moment is 7.47×10^5 N-mm. Using a transformed section method the maximum positive and negative flexural stresses at midspan are determined to be $\sigma_{\rm skin} = \pm 2.39$ MPa and $\sigma_{\rm core} = \pm 0.038$ MPa. The foam core shear stress is $\tau_{core} = 0.037$ MPa. Since the transverse strength properties of the SNLTriax layup are not provided it is assumed that first ply failure will occur in the $\pm 45^{\circ}$ plies and the ultimate tensile and compressive strengths for the skin in the transverse direction are therefore $\sigma_{\text{UTStrans}} = 144 \text{ MPa}$ and $\sigma_{\text{UCStrans}} = -213 \text{ MPa}$, respectively. The ultimate tensile and compressive strengths for the isotropic core are taken as $\sigma_{\rm UTS} = 3.1 \, \text{MPa}$ and $\sigma_{\rm UCS} = -3.8 \, \text{MPa}$, respectively and the shear strength of the core is taken as $\tau_U = 2.0 \text{ MPa} (\text{AIREX}^{\mathbb{R}} \text{ T92.200 thermoplas-}$ tic foam from 3A Composites). It can be seen that all stresses are well below the ultimate stress in the sandwich skin panel for this loading condition.

Case (2): The sandwich web panel consists of a 50 mm thick foam core and two 3 mm face skins of SNLBiax ($\pm 45^{\circ}$) glass fiber composite. $E_{L(biax)}$ =

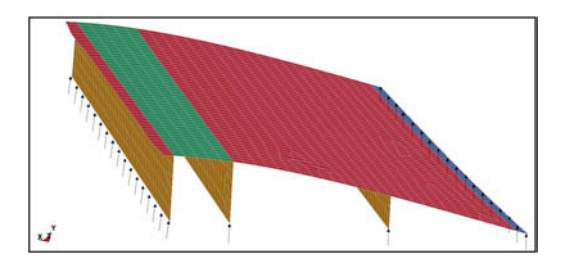


Figure 3. FEM mesh and boundary conditions.

 $13.6 \,\mathrm{GPa}$, $\mathrm{E_{foam}} = 0.256 \,\mathrm{GPa}$. The web height is 870 mm. The length of the web panel is taken as 7 m. The web is loaded by a tributary area of half the distance to web 2 on the left side and half the distance to web 3 on the right side. The web is considered to be simply supported at its two bottom ends (spanning between the end walls of the house) and not connected to the skin at its top edge (i.e., it is a simple rectangular thin deep beam and not a T-beam). The line load on the top of the web is calculated to be 2.01 N/mm and the maximum bending moment at midspan is determined to be $M_{max} = 1.23 \times 10^7$ N-mm. Using a transformed section method the maximum positive and negative flexural stresses at midspan are determined to be $\sigma_{\rm skin} = \pm 13.65 \, \text{MPa}$ and $\sigma_{\rm core} = \pm 0.257$ MPa. The shear stress core is $\tau_{core} = 0.2$ MPa. The ultimate tensile and compressive strengths for the skin are $\sigma_{\rm UTS} = 144 \, \text{MPa}$ and $\sigma_{\rm UCS} = -213 \, \text{MPa}$, respectively. Core properties are as in Case (1). It can be seen that all stresses are well below the ultimate stress in the sandwich web panel for this loading condition.

It should be noted that a more detailed analysis is needed to include local bucking of the skins and webs, failure at the skin/core interfaces and local bearing at the supports. Such calculations are better suited to numerical methods like the finite element method discussed in what follows. In addition, for structural (not aerospace or mechanical) engineering design calculations appropriate building code probability material/element resistance factors will need to be applied.

2.1.3 Finite element model of the roof frame

The finite element modeling of the roof frame was conducted using the implicit version of the LS-DYNA software code (www.lstc.com). Only stress analysis was conducted. The different segments of the roof frame that have distinct material properties and layups are shown in different colors in Fig. 3.

Green designates the CFRP/GFRP spar cap between webs 1 and 2 (5 mm SNLTriax/80 mm SNL-Carbon/5 mm SNLTriax), red the GFRP/foam shell sandwich panel (5 mm SNLTriax/60 mm foam/5 mm SNLTriax), dark blue the GFRP/foam trailing edge (TE) (5 mm SNLTriax/15 mm Glass UD/40mm Foam/5 mm SNLTriax), and brown the GFRP/foam web panels (3 mm SNLBiax/50 mm foam/3 mm SNL-Biax) (Griffith, 2013). A fully-integrated laminated shell element (LSDYNA ELFORM=16) was used. The

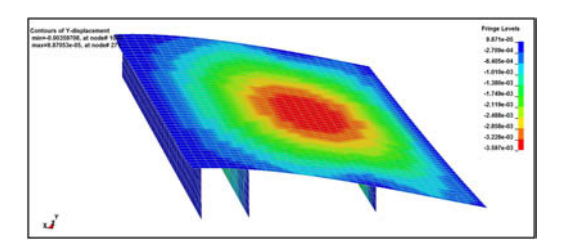


Figure 4. Displacement of the roof frame in the y-direction.

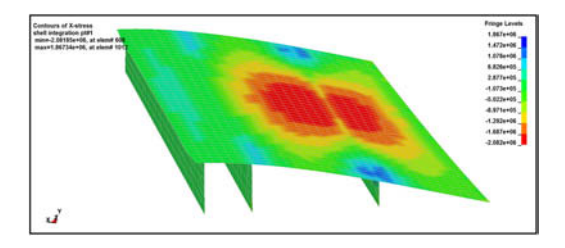


Figure 5. Stresses in top layer in x-direction (width).

total model consisted of 1813 elements. In the model the x and z coordinates are in the horizontal plane (in the 5 m width and 7 m length, respectively) and the y coordinate is perpendicular to this plane. The major 11-axis of the materials (see Table 1) is aligned with the blade longitudinal axis which is the z-direction in the FEM model.

The boundary conditions used in the FEM for the roof frame are shown in Fig. 3 by the vertical arrows (pinned in x, y and z directions). Webs 2 and 3 were pinned at the bottom of their long ends (to simulate bearing on the widthwise wall) and web 1 and the trailing edge were both pinned along their 7 m long edge (to simulate bearing along the entire lengthwise wall.)

2.1.4 Results of finite element analysis

Selected results from the finite element analyses are presented to illustrate the stress distributions and displacements in key directions. As in the hand calculations the applied gravity load (DL+LL) was 1.44 kN/m². Fig. 4 shows the vertical displacement (deflection) of the roof frame (in the y-direction).

As expected the maximum deflection (3.59 mm downwards) occurs near the center of the large center panel of the skin (shown in red). The two-way action of the shell can be seen. It is pin supported on all four sides and stiffened in the longitudinal direction by the interior webs. A very small uplift (0.0987 mm) (consistent with a SS plate) in the corners shown by the dark blue color can be seen.

The stresses at the top surface in the SNLTriax layer in the skin in the x-direction are shown in Fig. 5.

The red color shows the large compressive stress in the transverse (x or 22 direction). The maximum transverse compressive stress is 2.08 MPa. As can be seen web 3 provides some intermediate support and the compressive stress decreases along this line giving

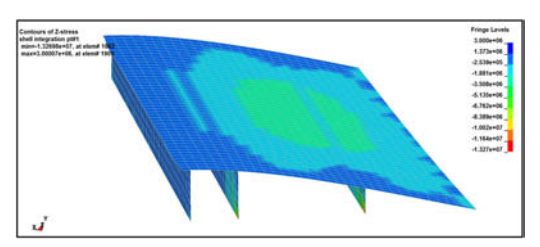


Figure 6. Stresses in top layer in z-direction (length).

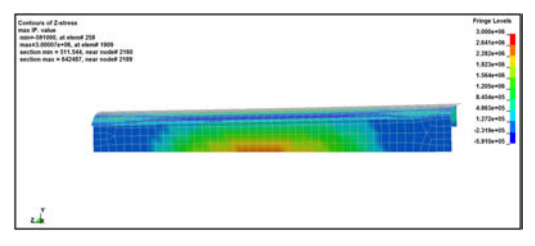


Figure 7. Stresses in web 2 in z-direction.

the butterfly shaped stress contours. The maximum transverse tensile stress in the SNLTriax skin in the x-direction at the underside of the shell is found to be 1.29 MPa (plot is not shown for this layer but is similar in shape). As can be seen the neutral axis of the shell is not at the shell midplane

The stress in the z-direction (longitudinal 7 m direction) in the top SNLTriax skin layer are shown in Fig. 6.

As with the x-direction the central portion is in compression (green) with a maximum longitudinal compressive stress in this region of 3.5 MPa. The remained of the top surface (aqua and light blue) show that the entire top surface stress in the longitudinal direction is compressive. The tensile stresses in the plot (dark blue) occur in web 1 at the bottom. Finally, the stresses in the middle web (web 2) are shown in Fig. 7.

Web 2 is pin supported at the bottom of its two ends. The web is in one-way bending with tension on the bottom and compression on the top. Due to the T-beam effect the compressive stress is distributed over the top panel and the web is primarily in tension throughout its depth (precluding buckling). The maximum longitudinal tensile stress in the SNLBiax skin layers at the bottom of the web is 3.0 MPa while the maximum longitudinal compressive stress at the top is only 0.591 MPa. In addition to the stresses in the skins of the top panel and the webs detailed above the stresses in the foam cores were also determined. The shear stresses in the core are listed in Table 2.

2.1.5 Comparison between hand calculation and FEM results

Table 2 lists the values of the stresses determined by hand calculation in 2.1.2 and the FEM stresses in 2.1.4. The ultimate stresses are also listed.

Table 2. Comparison between hand calculation and finite element method results and ultimate values

	Case (1	Case (1) shell panel			Case (2) middle web			
	Skin σ _{ten} MPa	Skin $\sigma_{ m comp}$ MPa	Core τ MPa	Skin σ _{ten} MPa	Skin σ _{comp} MPa	Core τ MPa		
Hand FEM Ultimate	2.39 1.29 144.0	2.39 2.08 213.0	0.040 0.034 2.0	13.65 3.00 144.0	13.65 0.59 213.0	0.200 0.067 2.0		

It can be seen that the results for the shell panel are quite similar. The hand calculation assumed one-way bending while the true behavior is two-way bending. However, in the middle of the panel far from the supports the panel response is close to one way behavior and therefore the results are close.

The results for the middle web are not as close due to the very simplifying assumption of ignoring the T-beam effect made for the hand calculations. Nevertheless, the stresses are of the same order of magnitude indicating that no gross errors were made in either the hand calculations or the FEM calculations.

3 CONCLUSION

This paper has demonstrated that conventional structural analysis of complex parts cut from large wind turbine blades is possible and that it is likely that the stress levels in the parts will be rather low for typical structural loads. Nevertheless, this is not trivial as blade models (if even available) need to be used with extreme caution. The blade tapers and twists and its material properties change along its length. For structural detailing a model showing the thickness of the blade is needed. However, most blade models used for aerodynamic and structural analysis are wire frame surface models. In addition for an actual infrastructure applications building codes will need to be used to determine appropriate load and resistance factors based on the residual properties of the decommissioned blade.

ACKNOWLEDGEMENT

Support for this research was provided by the U.S. National Science Foundation (NSF) under grants 1701413, and 1701694; by InvestNI/Department for the Economy (DfE) under grant 16/US/3334 and by Science Foundation Ireland (SFI) under grant USI-116 (US-Ireland Tripartite program).

REFERENCES

- Bank, L.C., Arias, F.R., Yazdanbakhsh, A., Gentry, T.R., Al-Haddad, T., Chen, J.F. & Morrow, R. 2018. Concepts for Reusing Composite Materials from Decommissioned Wind Turbine Blades in Affordable Housing. *Recycling*. 3(1).
- Berg, J.C. & Resor, B.R. 2012. Numerical Manufacturing and Design Tool (NuMAD v2.0) for Wind Turbine Blades: User's Guide. SAND2012-7028, Sandia National Laboratories, Albuquerque, NM, USA.
- Griffith, T. 2013. The SNL100-01 Blade: Carbon Design Studies for the Sandia 100-meter Blade. 2013. SAND2013-1178. Sandia National Laboratories, Albuquerque, NM, USA..
- Jensen, J.P. & Skelton, K. 2018. Wind turbine blade recycling: experiences, challenges and possibilities in a circular economy. Ren. & Sust. Energy Reviews. 97: 165–176.
- Job, S., Leeke, G., Mativenga, P.T., Oliveux, G., Pickering, S. & Shuaib, N.A. 2016. Composites Recycling: Where are we now? Composites UK Ltd, www.compositesuk.co.uk.
- Liu, P. & Barlow, C.Y. 2017. Wind turbine blade waste in 2050. Waste Management, 62: 229–240.
- Oliveux, G., Dandy, L., & Leeke, G. 2015. Current status of recycling of fibre reinforced polymers: Review of technologies, reuse and resulting properties. *Prog. in Mat. Sci.* 72: 61–99.
- Tasistro-Hart, B., Al-Haddad, T., Bank, L.C.& Gentry, T.R. 2019. Reconstruction of Wind Turbine Blade Geometry and Internal Structure from Point Cloud Data. The 2019 ASCE International Conference on Computing in Civil Engineering, June 17–19, 2019, Georgia Institute of Technology, Atlanta, GA, USA.
- Yazdanbakhsh A. & Bank, L.C. 2014. A Critical Review of Research on Reuse of Mechanically Recycled FRP Production and End-of-Life Waste for Construction. *Polymers*, 6: 1810–1826.
- Yazdanbakhsh, A., Bank, L.C. & Tian, Y. 2018. Mechanical Processing of GFRP Waste into Large-Sized Pieces for Use in Concrete. Recycling. 3(1).